First-order nature of the spin-reorientation phase transition in $SmCrO_3$

Tusita Sau,[1] Shivani Sharma,[2] Poonam Yadav,[3] R. Baumbach,[4] T. Siegrist,[2,5] Alok Banerjee,[1] and N. P. Lalla[1]

[1]*UGC-DAE Consortium for Scientific Research, Indore-452001, India*

[2]*National High Magnetic Field Laboratory, Florida State University, Tallahassee, Florida 32310, USA*

[3]*IBS-CINAP, SungKyunKwan University, 2066 Seoburo, Jangan-gu, Suwon 16419, Republic of Korea*

[4]*Department of Physics, Florida State University, Tallahassee, Florida 32310, USA*

[5]*Department of Chemical and Biomedical Engineering, FAMU-FSU College of Engineering, Tallahassee, Florida 32310, USA*

(Received 26 April 2022; revised 13 July 2022; accepted 27 July 2022; published 10 August 2022)

The ever expected canted antiferromagnetic (CAFM) $Pb\prime n\prime m : \Gamma_4(\boldsymbol{G_x}, A_y, F_Z; F_Z^R)$ to $Pbn\prime m\prime : \Gamma_2(F_x, C_y, \boldsymbol{G_Z}; F_x^R, \boldsymbol{C_y^R})$ spin reorientation phase transition (SRPT) has only recently been confirmed through high-resolution time-of-flight neutron scattering studies by Sau *et al.* [Phys. Rev. B **103**, 144418 (2021)]. Despite several studies on $SmCrO_3$, the nature of its SRPT still remains debatable. In the present study, we revisit the issue through dc $M(T)$ and ac-susceptibility, $\chi_{ac}(T)$, measurements. Repeated cycle field-cooled-cooling and field-cooled-warming dc $M(T)$ measurements clearly expose a temperature point differentiating the regimes of continuous and discontinuous parts of the SRPT. The discontinuous part has a tiny but clear hysteresis in $M(T)$, confirming the first-order nature of the SRPT with supercooling (T^*) and superheating (T^{**}) temperatures to be ∼33 and ∼36 K, respectively. The hysteresis in the $M(T)$ is strongly supported by the occurrence of hysteresis in the nondispersing peaks in $\chi_{ac}(T)$, measured using a 3 Oe ac signal amplitude during cooling and heating under zero dc-bias. Below SRPT, the complete reversibility of $M(T)$ and $\chi_{ac}(T)$ confirms the second-order nature of the Sm^{3+} ordering at T_{N2}, which arises due to independent Sm^{3+}-Sm^{3+} interaction. Similarly, the absence of hysteresis in $M(T)$ as well as in $\chi_{ac}(T)$, across the paramagnetic to CAFM Γ_4 phase transition, proves the second-order nature of this phase transition.

DOI: 10.1103/PhysRevB.106.064413

I. INTRODUCTION

Due to the highly localized nature of rare earths (R's), f-electrons, the compounds that contain them, have always been a source of interesting physics at relatively low temperatures. It becomes more so if these moments happen to interact with the 3d-block transition-metal moments, which usually order at relatively high temperatures. Among many such compounds are the rare-earth and transition-metal-based magnetic distorted perovskites, including orthomanganites ($RMnO_3$) [1,2] and orthoferrites ($RFeO_3$) [3,4], which possess immense technological potential for magnetoelectric multiferroicity. In this series, the rare-earth orthochromites ($RCrO_3$) [5–7] are additionally interesting due to their coexisting functionalities comprising multiferroicity, spin reorientation phase transition (SRPT) [8–18], and magnetization reversal, which have the potential for possible novel applications in fast magnetic switching devices [19–21] and magnetic refrigeration [22]. The remarkable properties in these compounds arise out of polarization of the localized moments of R^{3+} ions under the internal field of Cr^{3+} moments, due to their antisymmetric superexchange and the underlying Dzyaloshinskii-Moriya (DM) interactions. The need for materials design to harness the maximum benefit out of novel functional properties, and the microscopic understanding of the basic physics behind the interactions, necessarily require an understanding of the true nature and order of the SRPT. This is also likely to resolve the possible role of magnetostructural coupling behind the SRPT. At this juncture it is worth mentioning that SRPT is also realized in thin films appearing as a function of film thickness [23].

Despite a plethora of studies on SRPT in different compounds [8–22], the nature of SRPT in $RCrO_3$ still remains debatable. In the family of $RCrO_3$, $SmCrO_3$ has been studied intensively, but reports of possible magnetoelectric multiferroic behavior [24,25] have attracted fresh attention. Similar to various other orthoferrites and orthochromates, $SmCrO_3$ also evolves from the paramagnetic state to a canted antiferromagnetic (CAFM) phase at $T_{N1} = 192$ K, and then SRPT at $T_{SRPT} = 34$ K. In most of these studies [8,26–29], the two transitions—CAFM and SRPT—are shown to possess $\Gamma_4(G_x, A_y, F_Z; F_Z^R)$ and $\Gamma_2(F_x, C_y, G_Z; F_x^R, C_y^R)$ spin configurations, respectively, except for $DyFeO_3$ and $NdCrO_3$ [30], which undergo Γ_4 to Γ_1 and Γ_2 to Γ_1 transformations across the respective SRPTs. The correct spin configurations of $SmCrO_3$ across the CAFM and SRPT have been recently confirmed to be $\Gamma_4(\boldsymbol{G_x}, A_y, F_Z; \boldsymbol{F_Z^R})$ and $\Gamma_2(F_x, C_y, \boldsymbol{G_Z}; F_x^R, C_y^R)$, respectively, by Sau *et al.* [31] using magnetic neutron scattering. A diagrammatic view of the magnetic structure revealing the change in the orientations of the Cr^{3+} and Sm^{3+} moments across the SRPT has been shown in Figs. 1(a) and 1(b).

Initially the SRPT was understood following the phenomenological description by Horner and Verma [9] as the

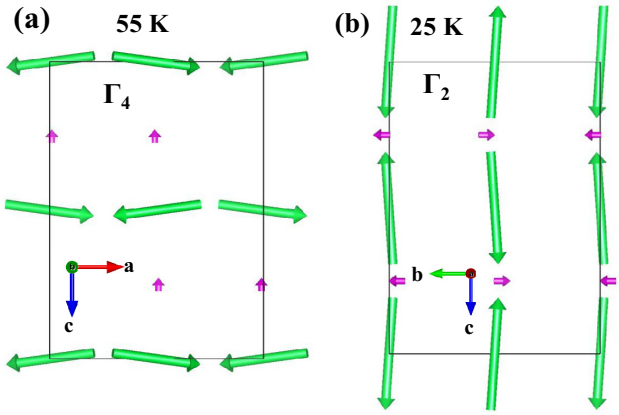

FIG. 1. Magnetic struture of (a) Γ_4 phase at 55 K and (b) Γ_2 phase at 25 K. It may be noted that in Γ_4 phase the magnetic structure of Cr moments is G_X-type AFM with Cr moments oriented mostly along the x-axis and that of Sm is F_Z-type, with Sm moments aligned along the z-axis. After SRPT, i.e., in Γ_2 phase, the magnetic structure of Cr moments still remains G-type AFM but now the Cr moments get flipped along the Z-axis and that of Sm is C-type AFM with moments aligned along the Y-axis.

easy-axis rotation arising from the temperature dependence of the *second* (K_1) and *fourth*-order (K_2) single-ion magnetic anisotropy coefficients [32] as given in (1),

$$E = K_0 + K_1 \sin^2\theta + K_2 \sin^4\theta. \quad (1)$$

This has been found to be followed in $Mn_{2-x}Cr_xSb$ [33]. It has been theoretically [34] and experimentally [35,36] shown that the SRPT does arise due to the fourth-order anisotropy term (K_2), which is generally small, but it dominates the orientation behavior when the second-order anisotropy term (K_1) changes sign with temperature [8,37,38] and when K_2 is negative, an abrupt jump of spins signifying that a first-order phase transition takes place. Levinson *et al.* [39] have also shown that SRPTs may be of both characters, i.e., either showing a second-order phase transition (SOPT) or a first-order phase transition (FOPT).

However, keeping in mind the experimentally observed fact regarding SRPT, namely that it is seen only for those rare-earth ferrites and chromates whose rare-earth ions are magnetic [8,10], a proper approach necessarily demands two-ion anisotropy, while the theory of Horner and Verma [9] is based on single-ion anisotropy. Therefore, as such this appears incompatible for the rare-earth orthoferrites and orthochromates. As pointed out by Yamaguchi [10], for Cr^{3+} ($S = 3/2$) the fourth-order anisotropy K_2 is nonexistent, and therefore the Horner and Verma [9] theory is technically incompatible for the SRPT observed for $RCrO_3$ compounds. Yamaguchi [10] thought the SRPT was a result of both antisymmetric and anisotropic-symmetric exchange interactions between M^{3+} and R^{3+} spins, which supposedly could better define the phenomenon of SRPT.

Experimentally, the nature of SRPT in $SmCrO_3$ was first studied by Gorodetsky *et al.* [40] using sound velocity measurements on single crystals, and despite the above-discussed facts related to the incompatibility of Horner and Verma [9] theory for rare-earth chromates, Gorodetsky *et al.* attributed it to a second-order phase transition following the same sound velocity measurements. Despite the fact that fourth-order anisotropy K_2 is nonexistent for Cr^{3+}, Gorodetsky *et al.* simply delivered a very short argument about the appearance of a finite moment at Sm^{3+}, whereas their detailed interpretation of the observation was based on the approximation considering the nonexistence of rare-earth moments.

All of the above-mentioned facts indicate that there is still sufficient room to revisit the true nature of the SRPT in $SmCrO_3$, which has not been attempted in the recent past after the work of Gorodetsky *et al.* [40]. Only recently, Tripathi *et al.* [41] attempted to probe it in $SmCrO_3$ as the FOPT through phase-coexistence studies using neutron scattering, but due to improper structure refinement of the NPD data, that study remained inconclusive.

According to Landau's phenomenological theory, presented for first-order and second-order phase transitions [42], the nature (first or second) of a temperature-driven phase transition can be confirmed directly, and more concretely, through the temperature dependence of the related order parameters measured during cooling and heating cycles. The theory of FOPT incorporates the double-well potential, which requires that the order-parameter variation as a function of temperature must show hysteresis across the FOPT. The absence of hysteresis is usually taken as a signature of an SOPT. As far as the sharpness of the order-parameter variation against temperature in a FOPT is concerned, it may be affected by the sample's structural quality. Disorder can broaden an FOPT [43] and in acute cases it may even be mistaken as a second-order transition. The absence of hysteresis thus may prevent the confirmation of a SOPT, but the occurrence of hysteresis invariably confirms the presence of an FOPT. For magnetic phase transitions, the order parameter is magnetization (M), which can be measured very accurately yielding precise and reproducible data as a function of temperature $M(T)$ and/or magnetic field $M(H)$. In the present study, we revisited the nature of the SRPT in $SmCrO_3$ via detailed dc- and ac-susceptibility (χ_{ac}) measurements. Our magnetization results show the nature of the SRPT to be first-order, and the other two AFM transitions at T_{N1} and T_{N2} are shown to be second-order.

II. EXPERIMENT

Polycrystalline $SmCrO_3$ was synthesized following the solid-state route as described in Ref. [31]. After confirming the single-phase nature of the as-prepared $SmCrO_3$, the temperature dependence of the dc-magnetization $M(T)$ and the ac-susceptibility $\chi_{ac}(T)$ were measured down to 2 K using a SQUID magnetometer MPMS3 (Quantum Design Inc., USA) on an ~35 mg sample. Both measurements were done in settled mode with an effective wait time of about a few minutes per data point [44]. The $M(T)$ curves were measured under various protocols, such as zero-field-cooled (ZFC), field-cooled-cooling (FCC), and field-cooled-warming (FCW) at 20, 50, 500, and 1500 Oe. The $\chi_{ac}(T)$ curves were measured at various frequencies during cooling and warming cycles. Isothermal magnetization, $M(H)$, curves were recorded at various temperatures. It is worth mentioning here that before

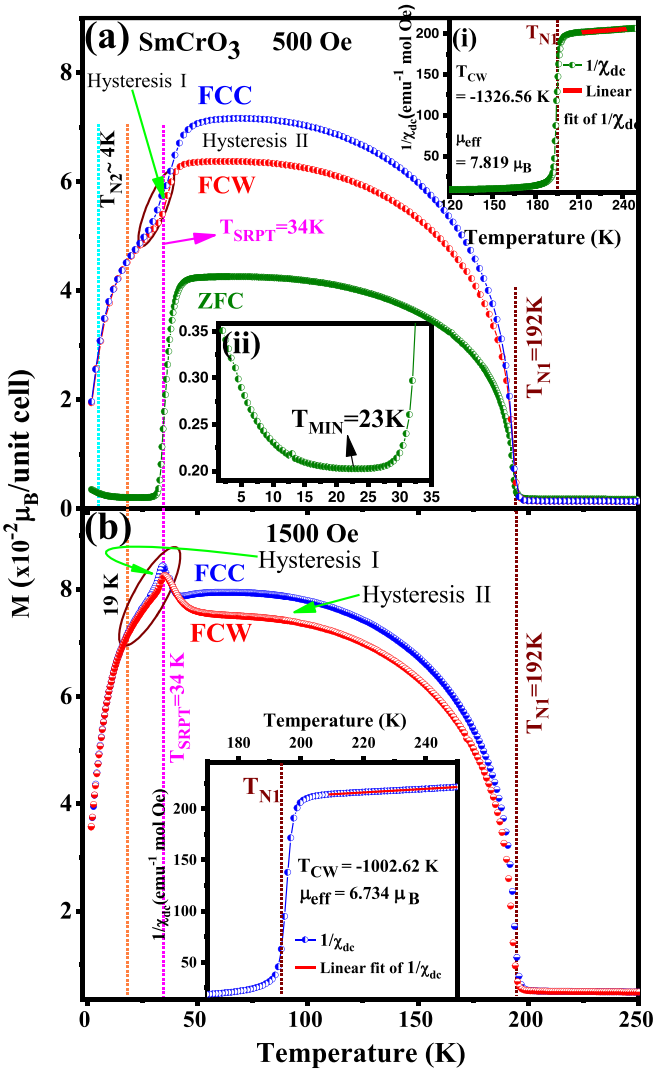

FIG. 2. (a) ZFC, FCC, and FCW dc $M(T)$ data of $SmCrO_3$ measured under 500 Oe, showing the occurrence of a weak-FM transition at 192 K arising due to CAFM ordering. The sharp drops in magnetization at ∼34 K and ∼19 K are due to SRPT and commencement of AFM ordering due to Sm-Sm direct interaction. The insets show the corresponding CW-fit and variation of ZFC magnetization.

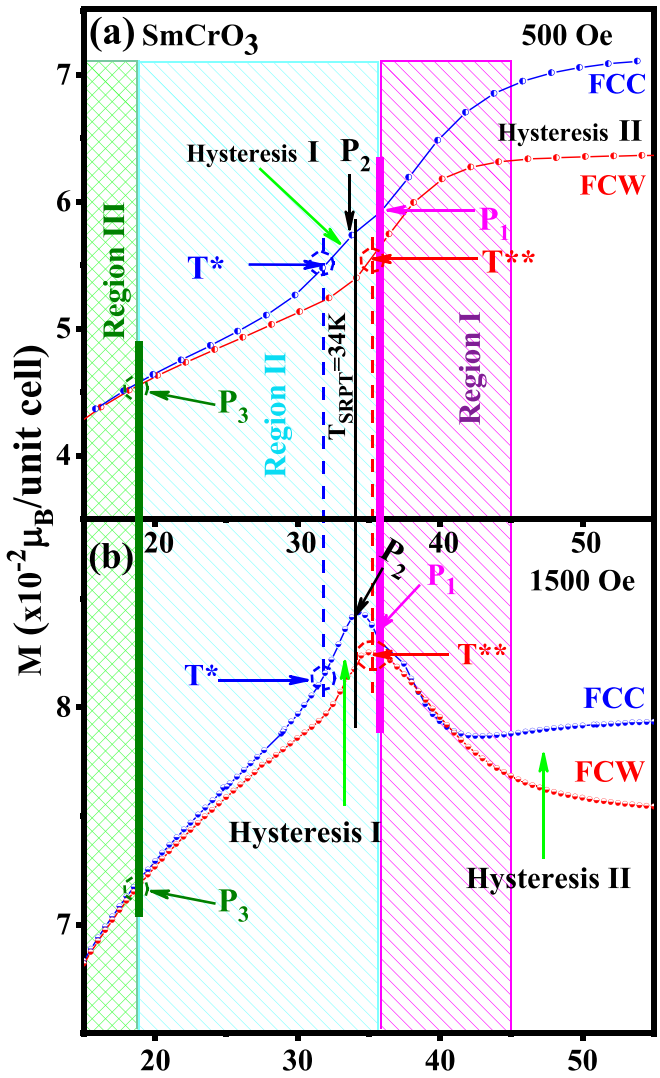

FIG. 3. Enlarged view of the FCC and FCW dc-magnetization variations across SRPT in $SmCrO_3$ measured under (a) 500 Oe and (b) 1500 Oe. This highlights the presence of hysteresis in the dc $M(T)$ confirming to the first-order nature of the SRPT. The superheating (T^{**})/supercooling (T^{*}) temperatures have been indicated.

performing ZFC measurements, the remnant field inside the SQUID was carefully zeroed, either by soft-quenching the magnet or by oscillating the field.

III. RESULTS AND DISCUSSIONS

The single-phase nature of the as-prepared $SmCrO_3$ sample was confirmed using x-ray diffraction (XRD) as well as time-of-flight (TOF) neutron powder diffraction (NPD) measurements [31]. RT-XRD and TOF-NPD data of the as-prepared $SmCrO_3$ sample were Rietveld-refined using *Pbnm* space group. The Wyckoff positions of Sm, Cr, and the two oxygen atoms O1 and O2 were confirmed to occupy a *Pbnm* structure as reported in Ref. [31].

Figures 2(a) and 2(b) show the temperature dependence of the dc-magnetization, $M(T)$, of $SmCrO_3$ measured, respectively, at 500 and 1500 Oe fields. A sharp rise in the magnetization below $T_{N1} = 192$ K, slowly approaching maxima of ∼0.071 μ_B/u.c. (unit cell) (at 500 Oe) to 0.079 μ_B/u.c. (at 1500 Oe) at further low temperatures (∼62 K), indicates a weak-ferromagnetic (FM) transition. In the literature [45,46], such weak FM components are invariably attributed to the DM interactions [47,48], leading to CAFM ordering of Cr^{3+} moments. At T_{N1}, the Sm^{3+} moments remain paramagnetic. However, with decreasing temperature the Sm^{3+} moments slowly get polarized under the exchange field of Cr^{3+} [31]. This polarization is usually AFM in nature and known [8,10,49,50] to initiate continuous rotation of the Cr^{3+} moments leading to SRPT at ∼34 K, as shown in Figs. 2(a) and 2(b). The Curie-Weiss (CW) fit of the $(1/\chi_{dc}) - T$ data, measured at 500 Oe field, gives an effective moment (μ_{eff}) of 7.8 μ_b with $T_{CW} = -1323$ K; see the inset (i) of Fig. 2(a). On the other hand, the μ_{eff} and T_{CW}, as determined using the 1500 Oe $(1/\chi_{dc}) - T$, are found to be 6.7 μ_b and

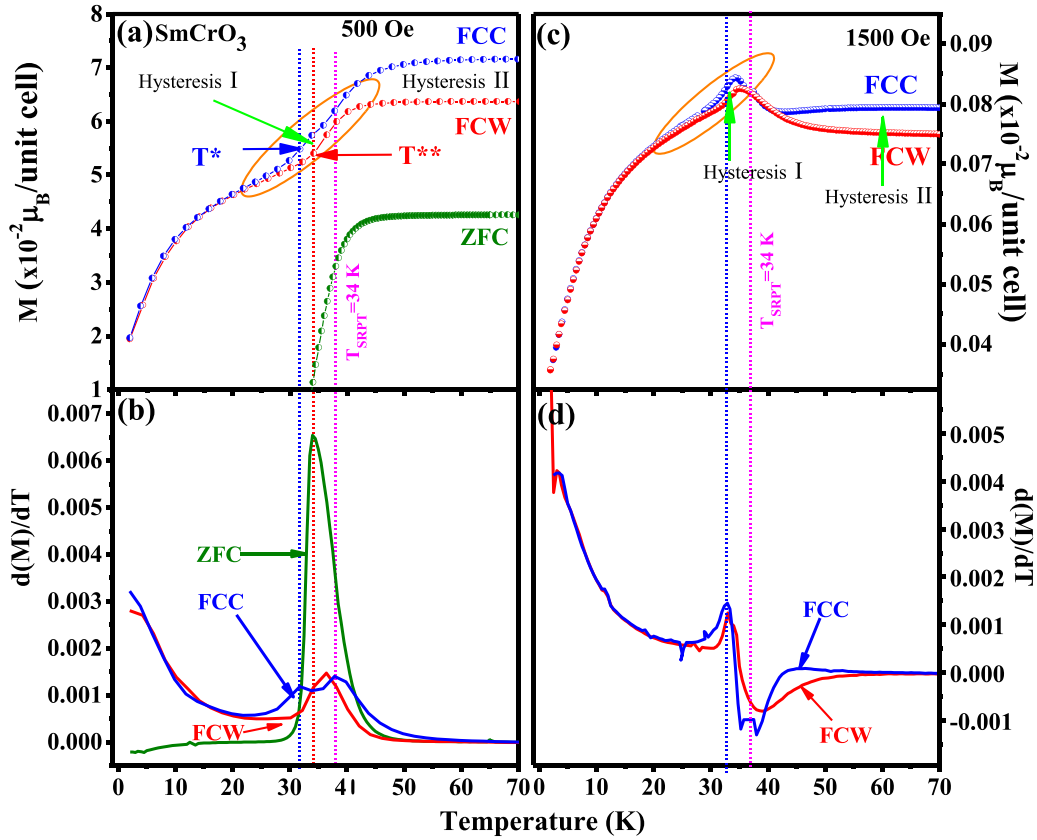

FIG. 4. The ZFC, FCC, and FCW M(T)s measured at (a) 500 Oe and (c) 1500 Oe fields. The corresponding first-derivative (dM/dT) curves (b) 500 Oe and (d) 1500 Oe bring out the fine features across the SRPT.

−1002 K, respectively; see the inset of Fig. 2(b). It shows that μ_{eff} of $SmCrO_3$ is slightly field-dependent. The order of magnitude of the presently determined μ_{eff} is in agreement with the previously reported ones [5,51]. However, the experimentally measured value of μ_{eff} is much larger as compared to the expected μ_{eff}, calculated for $SmCrO_3$ based on the individual moments of Cr^{3+} and Sm^{3+}. The large negative value of T_{CW} confirms the strong AFM interaction in $SmCrO_3$.

The ZFC $M(T)$, as shown in Fig. 2(a), undergoes a single sharp drop during SRPT. However, the FCC and FCW curves split into different components in different temperature regions around the SRPT. This can be better realized in the enlarged view of the dc $M(T)$ curves, as shown in Figs. 3(a) and 3(b), and also by the first derivatives of the dc $M(T)$, as shown in Figs. 4(a)–4(d). The FCC and FCW $M(T)$'s around SRPT can be broadly split in three different components as shown in Figs. 3(a) and 3(b) by differently hatched regions on a temperature scale. The $M(T)$ variations corresponding to 500 and 1500 Oe, despite looking different, have common features coincident on the temperature scale, as indicated by P_1, P_2, and P_3. Two of the features, P_1 and P_2, lie close to the SRPT in region II, while the third one, P_3, appears close to the boundary of regions I and II at ∼19 K. The FCC/FCW $M(T)$'s remain exactly reversible until below P_3 (i.e., below 19 K). But above P_3, the $M(T)$'s follow irreversible paths featuring two hystereses, marked as hysteresis I and II. The ∼4-K-wide hysteresis I, lying in region II, embodies the SRPT. But hysteresis II, starting in region I, bears a width of ∼155 K and extends much above the SRPT and finally merges at T_{N1}. For hysteresis I corresponding to 1500 Oe $M(T)$, the $M(T)$ varies differently in the pre-SRPT region as compared to that of 500 Oe. For that of 1500 Oe, the $M(T)$ first increases and then drops sharply at the SRPT ∼33 K. The above-described FCC and FCW $M(T)$'s measured on $SmCrO_3$ have revealed new features related to the SRPT, which were otherwise hidden in the ZFC data. As is discussed in the following, these observations are likely to change the existing understanding about the nature of SRPT in $SmCrO_3$ [10,40].

As shown in Figs. 3(a) and 3(b), the $M(T)$ curves, for 500 and 1500 Oe, respectively, look different but their features around the SRPT bear a one-to-one correspondence, which has been identified by the change in curvature of the $M(T)$'s occurring at common temperatures. For 500 Oe, the $M(T)$ curve continuously decreases until the inception of tiny hysteresis at P_1 in region II, whereas for 1500 Oe, the $M(T)$ continuously increases until P_1 before the inception of the corresponding hysteresis I. These coincident features have been highlighted by the vertical dotted lines of different colors. These features indicate that the SRPT is reached in two steps. The first step of the transition comprises a continuous rotation of the moments until point P_1, i.e., a second-order-like phase transition, and in the second step, the Cr^{3+} moments undergo a discontinuous jump to an altogether different spin-configuration below the inception point P_2, finally accomplishing the net SRPT.

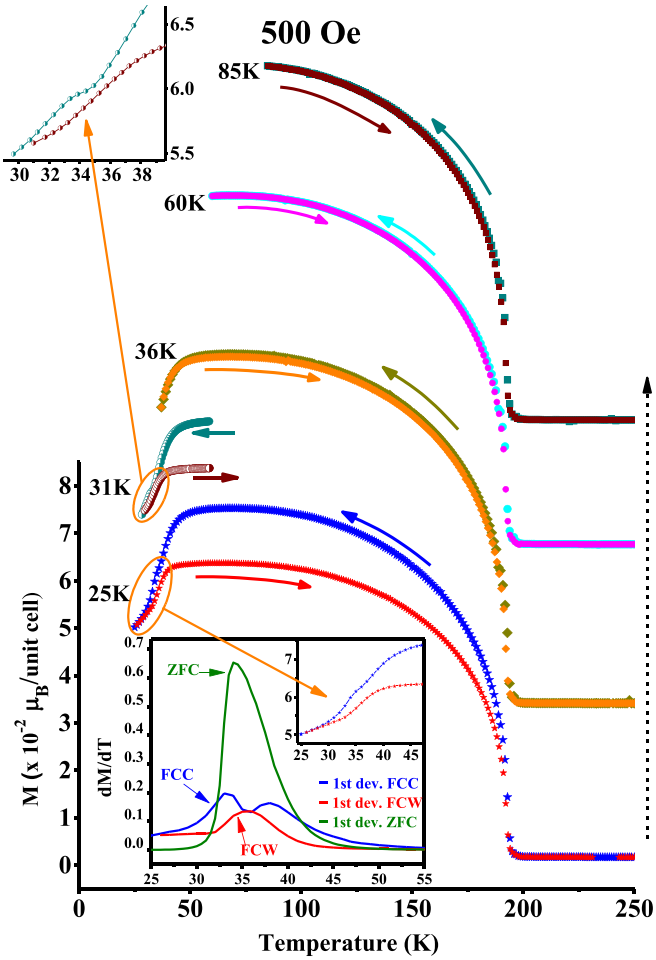

FIG. 5. A sequence of FCC and FCW $M(T)$ curves, all measured under 500 Oe field, while turning back for FCW at decreasingly lower temperatures of 85, 60, 36, 31, and 25 K. It depicts complete reversibility until 36 K, but below that, e.g., at ∼31 K, it becomes irreversible. The inset shows the first derivatives (dM/dT) of the $M(T)$ curves measured until 25 K. The splitting of the FCC curve across SRPT is quite evident from the first-derivatives curves.

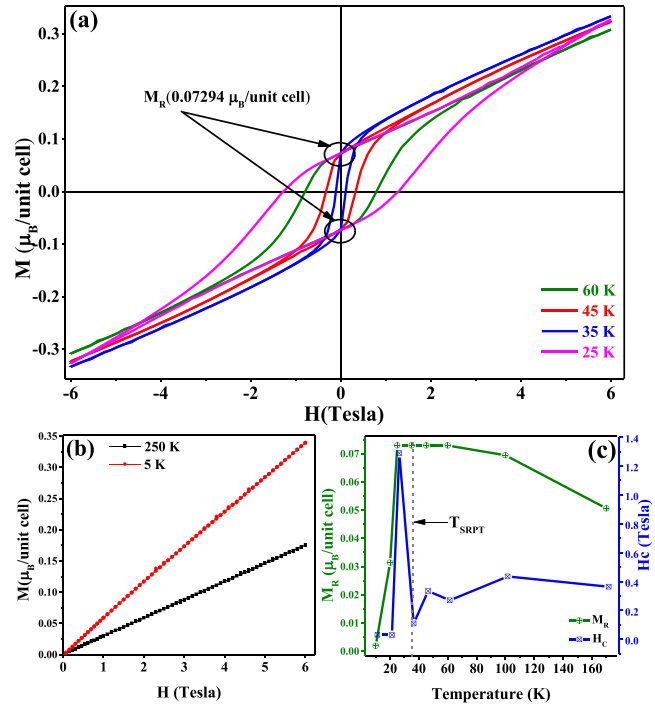

FIG. 6. Isothermal magnetization curves, $M(H)$, measured for $SmCrO_3$ at (a) 60, 45, 35, and 25 K; and (b) 250 and 5 K. (c) The temperature variation of the coercive-field (H_C) and the remanent-magnetization (M_R) as derived form the $M(H)$ loops.

To confirm the existence of such an inception point, we carried out a series of FCC and FCW $M(T)$ measurements at 500 Oe. Each set of FCC/FCW $M(T)$ was started from 250 K and then cooled down, respectively, to 85, 60, 36, 31, and 25 K; see Fig. 5. From Fig. 5, it is quite clear that until 36 K, at which the feature P_1 in the FCC $M(T)$ appears, the $M(T)$ remains totally reversible, and no sign of any broad (155-K-wide) hysteresis II is observed. This indicates a second-order-type continuous rotation. But as we go below 36 K, e.g., down to 31 K, the $M(T)$ curve becomes irreversible and the hysteresis I and II emerge. This measurement clearly proves the existence of a critical temperature, in between 36 and 31, below which the SRPT becomes irreversible.

The continuous variation of $M(T)$ in the pre-SRPT region is another interesting feature that has been investigated closely. The $M(T)$ corresponding to 500 Oe decreases slowly below ∼60 K, and only below ∼45 K does it take a deep downturn. On the other hand, the 1500 Oe $M(T)$ varies differently. In this case, the decreasing trend slowly diminishes, and below ∼45 K the magnetization gradually takes an upturn with a kink at $P_1 = 36$ K. This field dependence in the nature of net $M(T)$ in the pre-SRPT region appears due to competition between the temperature dependence of the domain magnetization of the ferrimagnetic Γ_4 phase and the strength of the antiparallel polarization of the Sm^{3+} moments against the exchange-field of ferrimagnetic order of the Cr^{3+} moments. The Γ_4 phase bears easy-plane magnetocrystalline anisotropy, which basically keeps decreasing towards the SRPT. This decrease is quite evident from the decreasing coercive-field H_c in different $M(H)$ loops of $SmCrO_3$ across the SRPT down to 35 K; see Figs. 6(a)–6(c). Below a critical measuring field, the ferrimagnetic domain magnetization remains low enough with respect to the antiparallel polarization of Sm^{3+} moments, and therefore the net magnetization remains overwhelmed by the antiparallel polarization of Sm^{3+} moments, and $M(T)$ keeps decreasing. Since $SmCrO_3$ becomes magnetically soft towards SRPT, at higher measuring fields the ferrimagnetic domain magnetization exceeds the opposition of the antiparallel polarization effect of Sm^{3+} moments and overwhelms the net magnetization, and keeps it increasing until the SRPT. Despite the differences in the pre-SRPT $M(T)$ at different measuring fields, the sharp drop in magnetization at the SRPT remains identical at both measuring fields. It signifies that SRPT is effectively governed by a change in the nature of magnetocrystalline anisotropy with respect to temperature, which owes its origin to the anisotropic superexchange interaction between Cr^{3+} and Sm^{3+} moments.

In Figs. 6(a)–6(c), the presence of a closed $M(H)$ loop with linear $M(H)$ at high fields typically signifies the

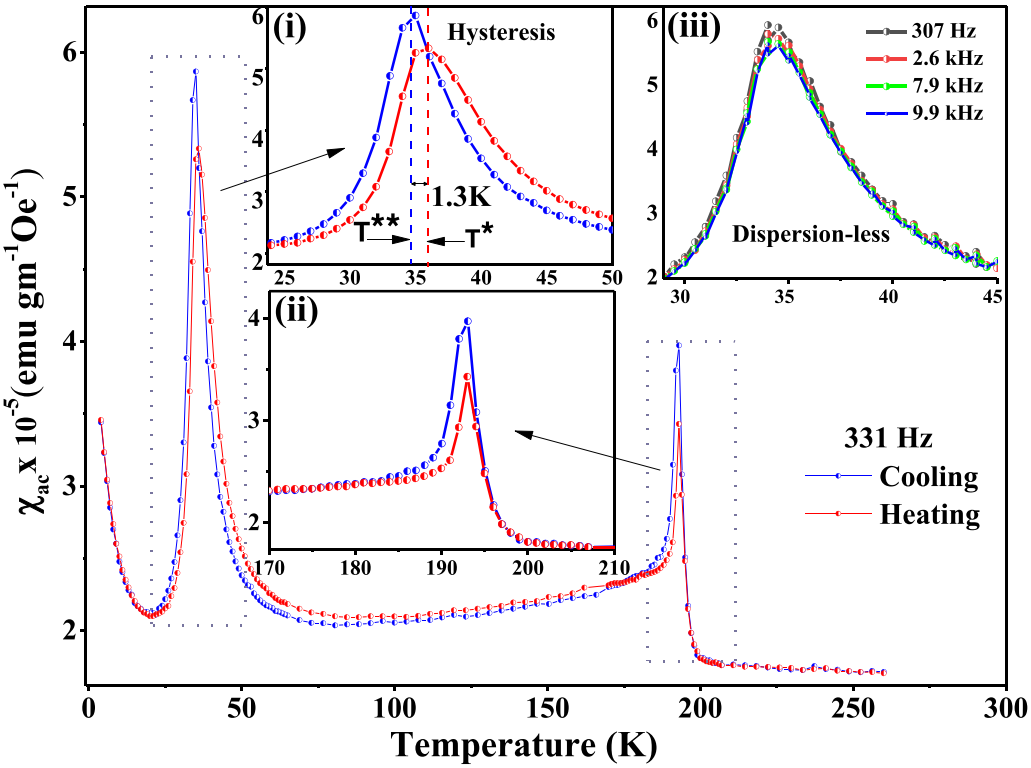

FIG. 7. $\chi_{ac}(T)$ of $SmCrO_3$ measured at 331 Hz during a heating-cooling cycle in the range of 4–260 K. Inset (i) highlights the occurrence of ∼1.3-K-wide hysteresis in $\chi_{ac}(T)$ across the SRPT. Inset (ii) shows that the transition from paramagnetic to CAFM and back to paramagnetic phase both exactly match at $T_{N1} = 192$ K. This asserts the second-order nature of the CAFM transition. Inset (iii) shows a complete absence of frequency dispersion of the $\chi_{ac}(T)$ peak corresponding to SRPT, confirming its thermodynamic nature.

coexistence of FM and AFM interactions. The closed-loop feature corresponds to the FM, and the linear behavior to the AFM interaction as confirmed via neutron scattering [31]. Figure 6(c) shows that the remanence magnetization (M_R) of $M(H)$ increases slowly, and across SRPT, from 60 to 25 K, it remains constant and below 25 K it drops nearly to zero, at ∼5 K. The $M(H)$ at 250 K, i.e., above T_{N1}, is linear due to the paramagnetic nature of the phase. At very low temperatures, at 5 K, it is once again linear, representing a pure AFM phase. The decreasing coercive-field in the $M(H)$ loops across SRPT is direct evidence of decreasing second-order magnetic anisotropy. Even at higher field, the Sm^{3+} moments keep maintaining its antiparallel alignment with the exchange-field of ordered Cr^{3+} moments. This process continues, leading to a ∼90° flip of the Cr^{3+} moments at the SRPT [10,31]. The much lower value of ZFC magnetization of Γ_2 phase is due to high uniaxial magnetic anisotropy of the Γ_2 phase as compared to the easy-plane anisotropy of the Γ_4 phase. Keeping in mind the fact that a magnetic field itself is a thermodynamic variable, the presence of a magnetic field in a significant amount may change the scenario of the expected second-order phase transition.

The difference in the nature of magnetization variation under FCC and FCW in Figs. 3(a) and 3(b) has thus revealed the true nature of the SRPT, which remained hidden in the ZFC data. The magnetization being the order parameter, the irreversibility with ∼4-K-wide hysteresis-I signifies the first-order nature of the SRPT with supercooling temperature $T^* = 33$ K and superheating temperature $T^{**} = 36$ K. The reversible drop in $M(T)$ below ∼19 K, in contrast to the ZFC, where the magnetization gradually increases with a decrease in temperature, is attributed to the commencement of independent G_z^R-type AFM ordering of Sm^{3+} at $T_{N2} < 4$ K.

The conventional magnetization measurement techniques do require a finite measuring field, but it can be very small. In principle, the applied field should be as low as possible to know the intrinsic magnetic behavior of the sample. But for having an analyzable signal, the applied field usually has a reasonably large value, in the range of 100 Oe or more. Due to the presence of the applied measuring field as a third thermodynamic variable, therefore, the conclusion of SRPT being a true FOPT against temperature may remain arguable. However, in ac-magnetic susceptibility measurement, by virtue of its requirement, the amplitude of the ac-field remains very low at ∼1 to 3 Oe, and thus the theoretical requirement, of a field approaching zero, is reasonably well satisfied. Keeping this in mind, $\chi_{ac}(T)$ measurements were also carried out at different frequencies during cooling-heating cycles, in stabilized temperature mode. The root-mean-square value of the applied ac-field was kept to 3 Oe. Figure 7 shows the $\chi_{ac}(T)$ variation of $SmCrO_3$ measured at 331 Hz during heating and cooling cycles in the range of 4–260 K. The sharp peaks in $\chi_{ac}(T)$, at ∼192 K and 34 K, correspond, respectively, to CAFM and SRPT transitions. It should be noted that corresponding to the SRPT, the $\chi_{ac}(T)$ peaks appear at lower and higher temperatures, having ∼1.3 K hysteresis, respectively, during cooling and heating cycles; see inset (i) of Fig. 7. Keeping in mind the

fact that equally steeply varying portions of the heating and cooling $\chi_{ac}(T)$ curves, between 2 and 22 K, exactly match, the slow deviation of the heating $\chi_{ac}(T)$ curve from that of the cooling one above 22 K, while approaching SRPT, slowly deviates bringing out the observed 1.3 K difference. The hysteresis across the SRPT is genuine and represents the intrinsic characteristic of the sample. It may also be noted that the SRPT width is ∼30% larger during the heating cycle. The observed irreversibility in the temperature of the phase-transition during heating and cooling clearly characterizes the first-order nature of the SRPT. The 1.3 K hysteresis arises due to the difference in the superheating (T^{**}) and supercooling (T^{*}) temperatures of a FOPT. The inset (ii) of Fig. 7 highlights the exact match between the peak temperatures of $\chi_{ac}(T)$ corresponding to CAFM phase-transition, approving it to be a second-order phase transition. The absence of frequency-dispersion in $\chi_{ac}(T)$, as highlighted in inset (iii), proves that the peaks in $\chi_{ac}(T)$ correspond to the thermodynamic nature of the SRPT. Thus, the $\chi_{ac}(T)$ variation is also in full accordance with the dc $M(T)$, and thus confirms the first-order nature of the SRPT.

The hysteresis-II feature of the $M(T)$, corresponding to an ∼155-K-wide Γ_4 phase regime, is not a feature of any phase-transition, but rather is a result of two different paths of approaching the Γ_4 phase transformation. Figures 8(a)–8(c) show that the area under the FCC and FCW decreases as the measuring field increases. During the FCC cycle, the Γ_4 phase forms due to a disorder-order transition under an applied field, and relatively larger ferrimagnetic domains with higher domain-magnetization form due to the presence of the field. On the other hand, during FCW, the Γ_4 phase forms due to order-order transformation of the Γ_2 phase under an applied magnetic field. The definition of the preexisting domains in the Γ_2 phase will necessarily modify the 180° domains of the ferrimagnetic phase to minimize the magnetostatic energy. The increased number of 180° domains [31] will therefore lower the net magnetization. However, at higher measuring fields, more 180° domains will now align with the applied field, and net FCW magnetization will be close to that of the FCC, minimizing the difference. Finally, all such 180° domains vanish towards Γ_4 to the paramagnetic phase-transition, and the FCW $M(T)$ ultimately merges with the FCCM(T) at T_{N1}.

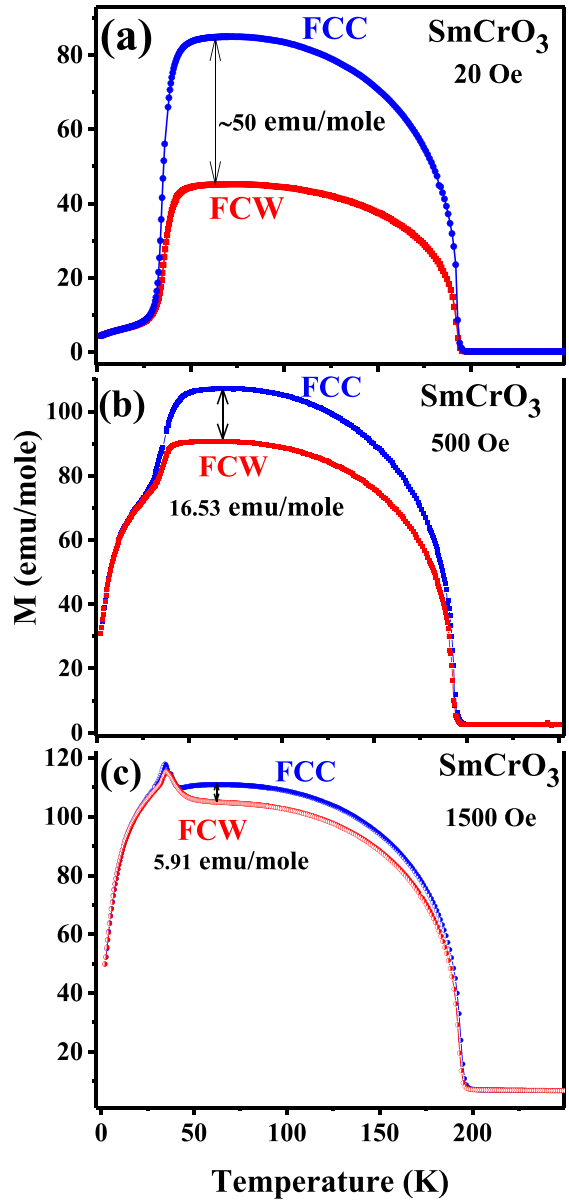

FIG. 8. $M(T)$ variations of $SmCrO_3$ measured at different fields. It is clearly shown that at higher measuring fields, the hysteresis-II feature keeps slowly diminishing.

IV. CONCLUSION

Based on the above-described results of dc and ac magnetization studies across various phase transitions in $SmCrO_3$, and the ensuing discussions, we conclude that observed spin-reorientation in $SmCrO_3$ is a result of two closely lying transitions. While cooling, the Cr^{3+} moments Γ_4 phase undergo a continuous rotation until ∼36 K following a second-order-type behavior, but below ∼33 K the Cr^{3+} moments undergo a discontinuous jump of first-order type to an altogether different spin-configuration of Γ_2 phase. The observed hysteresis-I feature in $M(T)$ and $\chi_{ac}(T)$, around the SRPT, is basically due to the first-order nature of the spin-configuration change. The wide hysteresis-II feature above the SRPT is due to different paths of the Γ_4 phase formation during cooling and heating cycles.

ACKNOWLEDGMENTS

The authors gratefully acknowledge Rajeev Rawat and Rajamani Raghunathan for helpful discussions on magnetism, and Kranti Kumar for magnetization measurements. Some of the magnetization measurements were performed at the National High Magnetic Field Laboratory, which is supported by the National Science Foundation Cooperative Agreement No. DMR-1644779 and the State of Florida.

[1] T. Kimura, T. Goto, H. Shintani, K. Ishizaka, T. Arima, and Y. Tokura, Nature (London) **426**, 55 (2003).

[2] T. Kimura, G. Lawes, T. Goto, Y. Tokura, and A. P. Ramirez, Phys. Rev. B **71**, 224425 (2005).

[3] Y. Tokunaga, S. Iguchi, T. Arima, and Y. Tokura, Phys. Rev. Lett. **101**, 097205 (2008).

[4] T. Yamaguchi and K. Tsushima, Phys. Rev. B **8**, 5187 (1973).

[5] B. Rajeswaran, D. I. Khomskii, A. K. Zvezdin, C. N. R. Rao, and A. Sundaresan, Phys. Rev. B **86**, 214409 (2012).

[6] S. Mahana, B. Rakshit, R. Basu, S. Dhara, B. Joseph, U. Manju, S. D. Mahanti, and D. Topwal, Phys. Rev. B **96**, 104106 (2017).

[7] S. Mahana, U. Manju, P. Nandi, E. Welter, K. R. Priolkar, and D. Topwal, Phys. Rev. B **97**, 224107 (2018).

[8] R. L. White, J. Appl. Phys. **40**, 1061 (1969).

[9] H. Homer and C. M. Varma, Phys. Rev. Lett. **20**, 845 (1968).

[10] T. Yamaguchi, J. Phys. Chem. Solids **35**, 479 (1974).

[11] K. Yoshii, J. Solid State Chem. **159**, 204 (2001).

[12] K. Yoshii, Mater. Res. Bull. **47**, 3243 (2012).

[13] H. J. Zhao, J. Íñiguez, X. M. Chen, and L. Bellaiche, Phys. Rev. B **93**, 014417 (2016).

[14] A. Durán, R. Escamilla, R. Escudero, F. Morales, and E. Verdín, Phys. Rev. Materials **2**, 014409 (2018).

[15] A. Kumar and S. M. Yusuf, Phys. Rep. **556**, 1 (2015).

[16] S. Biswas and S. Pal, Rev. Adv. Mater. Sci. **53**, 206 (2018).

[17] L. H. Yin, J. Yang, X. C. Kan, W. H. Song, J. M. Dai, and Y. P. Sun, J. Appl. Phys. **117**, 133901 (2015).

[18] N. Kumar and A. Sundaresan, Solid State Commun. **150**, 1162 (2010).

[19] Y. Cao, S. Cao, W. Ren, Z. Feng, S. Yuan, B. Kang, B. Lu, and J. Zhang, Appl. Phys. Lett. **104**, 232405 (2014).

[20] Y. K. Jeong, J.-H. Lee, S.-J. Ahn, and H. M. Jang, Solid State Commun. **152**, 1112 (2012).

[21] A. Kimel, B. Ivanov, R. Pisarev, P. Usachev, A. Kirilyuk, and T. Rasing, Nat. Phys. **5**, 727 (2009).

[22] M. Shao, S. Cao, S. Yuan, J. Shang, B. Kang, B. Lu, and J. Zhang, Appl. Phys. Lett. **100**, 222404 (2012).

[23] H. Fritzsche, J. Kohlhepp, H. J. Elmers, and U. Gradmann, Phys. Rev. B **49**, 15665 (1994).

[24] A. Ghosh, K. Dey, M. Chakraborty, S. Majumdar, and S. Giri, Europhys. Lett. **107**, 47012 (2014).

[25] G. N. P. Oliveira, R. C. Teixeira, R. P. Moreira, J. G. Correia, J. P. Araújo, and A. M. L. Lopes, Sci. Rep. **10**, 4686 (2020).

[26] E. F. Bertaut, G. Bassi, G. Buisson, P. Burlet, J. Chappert, A. Delapalme, J. Mareschal, G. Roult, R. Aleonard, R. Pauthenet *et al.*, J. Appl. Phys. **37**, 1038 (1966).

[27] E. F. Bertaut and J. Mareschal, Solid State Commun. **5**, 93 (1967).

[28] E. F. Bertaut, Acta Crystallogr. A **24**, 217 (1968).

[29] N. Shamir, H. Shaked, and S. Shtrikman, Phys. Rev. B **24**, 6642 (1981).

[30] R. D. Pierce, R. Wolfe, and L. G. Van Uitert, J. Appl. Phys. **40**, 1241 (1969).

[31] T. Sau, P. Yadav, S. Sharma, R. Raghunathan, P. Manuel, V. Petricek, U. P. Deshpande, and N. P. Lalla, Phys. Rev. B **103**, 144418 (2021).

[32] B. D. Cullity and C. D. Graham, *Introduction to Magnetic Materials*, 2nd ed. (John Wiley, New York, 2009), pp. 197–210.

[33] R. W. Houghton and W. Weyhmann, Phys. Rev. Lett. **20**, 842 (1968).

[34] G. F. Herrmann, Phys. Chem. Solids **24**, 597 (1963).

[35] F. B. Hagedorn and E. M. Gyorgy, Phys. Rev. **174**, 540 (1968).

[36] E. M. Gyorgy, J. P. Remeika, and F. B. Hagedorn, J. Appl. Phys. **39**, 1369 (1968).

[37] J.-S. Zhou, J. A. Alonso, V. Pomjakushin, J. B. Goodenough, Y. Ren, J.-Q. Yan, and J.-G. Cheng, Phys. Rev. B **81**, 214115 (2010).

[38] M. Taheri, F. S. Razavi, Z. Yamani, R. Flacau, P. G. Reuvekamp, A. Schulz, and R. K. Kremer, Phys. Rev. B **93**, 104414 (2016).

[39] L. M. Levinson, M. Luban, and S. Shtrikman, Phys. Rev. **187**, 715 (1969).

[40] G. Gorodetsky, R. Hornreich, S. Shaft, B. Sharon, A. Shaulov, and B. Wanklyn, Phys. Rev. B **16**, 515 (1977).

[41] M. Tripathi, R. J. Choudhary, and D. M. Phase, Phys. Rev. B **96**, 174421 (2017).

[42] L. D. Landau and E. M. Lifshitz, *Statistical Physics Vol. 5—Course of Theoretical Physics* (Pergamon, UK, 1976).

[43] Y. Imry and M. Wortis, Phys. Rev. B **19**, 3580 (1979).

[44] See Supplemental Material at http://link.aps.org/supplemental/10.1103/PhysRevB.106.064413 for the details of magnetic measurement, particularly of wait-time per data point.

[45] T. Morishita and K. Tsushima, Phys. Rev. B **24**, 341 (1981).

[46] S. Lei, L. Liu, C. Wang, C. Wang, D. Guo, S. Zeng, B. Cheng, Y. Xiao, and L. Zhou, J. Mater. Chem. **A1**, 11982 (2013).

[47] I. Dzyaloshinsky, J. Phys. Chem. Solids **4**, 241 (1958).

[48] T. Moriya, Phys. Rev. **120**, 91 (1960).

[49] L. Bellaiche, Z. Gui, and I. A. Kornev, J. Phys.: Condens. Matter **24**, 312201 (2012).

[50] D. I. Khomskii, J. Magn. Magn. Mater. **306**, 1 (2006).

[51] X. Qian, L. Chen, S. Cao, and J. Zhang, Solid State Commun. **195**, 21 (2014).